Int. J. Appl. Math. Comput. Sci., 2017, Vol. 27, No. 2, 323–336
DOI: 10.1515/amcs-2017-0023

amcs

COMPARATIVE CALCULATION OF THE FUEL–OPTIMAL OPERATING STRATEGY FOR DIESEL HYBRID RAILWAY VEHICLES

MAIK LESKA [a], HARALD ASCHEMANN [a,*], MICHAEL MELZER [b], MICHAEL MEINERT [b]

[a]Chair of Mechatronics
University of Rostock, Justus-von-Liebig-Weg 6, D-18059 Rostock, Germany
e-mail: Harald.Aschemann@uni-rostock.de

[b]Siemens AG
Werner-von-Siemens-Str. 65, 91052 Erlangen, Germany

In contrast to road-based traffic, the track as well as the corresponding duty cycle for railways are known beforehand, which represents a great advantage during the development of operating strategies for hybrid vehicles. Hence the benefits of hybrid vehicles regarding the fuel consumption can be exploited by means of an off-line optimisation. In this article, the fuel-optimal operating strategy is calculated for one specified track using two hybrid railway vehicles with different kinds of energy storage systems: on the one hand, a lithium-ion battery (high-energy storage) and, on the other, a double layer capacitor (high-power storage). For this purpose, control-oriented simulation models are developed for each architecture addressing the main effects contributing to the longitudinal dynamics of the power train. Based on these simulation models, the fuel-optimal operating strategy is calculated by two different approaches: Bellman's dynamic programming, a well-known approach in this field, and an innovative sensitivity-based optimisation.

Keywords: hybrid railway vehicle, fuel-optimal energy management, dynamic programming, sensitivity, optimisation.

1. Introduction

In Europe, only a certain part of the railway network is electrified. On the remaining lines the traffic is realised by diesel vehicles, e.g., diesel-multiple-units (DMUs). The rising ecological awareness, stricter emission and noise regulations, exhaust-free stations, and rising fuel prices lead the railway system suppliers worldwide to invest in the research and development of hybrid railway vehicles, which have a promising potential to reduce fuel consumption, emissions and noise. The most common hybrid vehicle uses an electric motor combined with an energy storage system to support the internal combustion engine (ICE). The choices of the energy storage system (ESS), further vehicle components and the overall propulsion chain depend on the vehicle's duty cycle and on other issues such as cost effectiveness as well as maintainability.

Hillmansen and Roberts (2007) carried out a kinematic analysis of ESSs suggesting a potential of up to 35% energy savings for commuter vehicles. The result of research work on hybrid concepts for diesel multiple units presented by Hillmansen *et al.* (2009) calculates a potential for the reduction in the fuel consumption of up to 25% on a fixed track. Beside the system architecture with its corresponding components and ESS, the operating strategy plays an important role regarding the fuel consumption of a hybrid vehicle (see Meinert *et al.*, 2015).

In the literature, many different optimal control strategies have been published in the past aiming at minimising the fuel consumption by managing the power flows of the energy sources. In particular, they can be classified into three groups (Pisu and Rizzoni, 2007):

1. dynamic programming (cf. Ogawa *et al.*, 2007; Brahma *et al.*, 2000);

2. rule-based approaches (cf. Dittus *et al.*, 2011; Torres *et al.*, 2014), fuzzy logic (see Wang and Yang, 2006; He *et al.*, 2013), and neural network control techniques (Moreno *et al.*, 2006);

*Corresponding author

3. methods based on the conversion of electric power into an equivalent fuel consumption (cf. Pisu and Rizzoni, 2007; Katranik, 2010).

Here, dynamic programming is the pre-dominant technique (see Bellman, 1952; 2003), which involves a discrete system model and discrete control variables to calculate the optimal management strategy. Based on the known duty cycles, the sequence of operating modes can be computed completely off-line. Moreover, also a fuel-optimal combined driving strategy and energy management can be determined using dynamic programming (see Leska and Aschemann, 2015).

In order to evaluate the total fuel and energy consumptions, respectively, the so-called tank-to-wheel (TTW) analysis is used, which deals with the energy conversion from the fuel and the electric capacity to the required mechanical energy at the wheels. The most common approach of the TTW analysis is the use of one lumped efficiency, which denotes the average value of the relation between the used fuel energy and the mechanical energy at the wheel (Guzzella, 2013). This so-called cycle-averaged efficiency is well suited for standard but not for hybrid vehicles. For this purpose, further methods like the use of two averaged efficiencies for the fuel-to-tank and the recuperation efficiency (cf. Ott *et al.*, 2012), and the use of several cycle-averaged efficiencies for each energy conversion step as in the work of Katrasnik *et al.* (2007) can be found in the literature. Leska *et al.* (2014) analyse the energy conversion using a complete simulation model of a hybrid railway vehicle with a mechanical transmission and an on-board lithium-ion battery including the main system components of the power train.

In this paper, the approach of Leska *et al.* (2014) is adapted for a hybrid railway vehicle with a diesel-electric transmission with a battery (Bat) and a double layer capacitor (DLC), respectively, as an on-board energy storage system (ESS). In Section 2, a control-oriented simulation model is derived for both railway vehicles. Then, the fuel-optimal operating strategy is calculated in two alternative ways: in Section 4.1 by dynamic programming according to Bellman, and in Section 4.2 by a sensitivity-based optimisation (cf. Leska *et al.*, 2014). Both the methods are compared with each other in Section 5 regarding accuracy, computational effort and the ability for an on-line energy management. Moreover, the impact of fuel costs regarding the overall life cycle costs is discussed. Finally, Section 6 concludes this article and provides an outlook on future research.

2. Modelling of a diesel-electric hybrid railway vehicle

The power train of a basic diesel-electric hybrid railway vehicle mainly consists of an internal combustion engine directly connected to an electric generator (G), an energy storage system (ESS) and an electric motor/generator (M/G) located on the drive shaft. In Fig. 1, a simplified structure of the modelled hybrid railway vehicle is presented. The ICE supplies the mechanical auxiliaries during the whole duty cycle. For the system architecture with a DLC, only mechanical auxiliaries are used, whereas for the architecture with a battery some of the consumers are electrified.

Given this system configuration, the following six operating modes are available:

- Mode 1: Pure ICE,
- Mode 2: Pure electric M/G,
- Mode 3: Boosting,
- Mode 4: Load level increase,
- Mode 5: Coasting,
- Mode 6: Recuperation.

In Mode 1, the ICE provides the total power demand. Mode 2 is a pure electric mode, where only the M/G is active. In Mode 3, the power boost mode, the power for the electric motor is supplied by the ICE via the generator and by the ESS. During a load level increase (Mode 4), the ICE provides more power than required to follow the pre-specified duty cycle. Here, the excess power is used for recharging the ESS. This mode is also used at standstill to fully recharge the ESS. In Mode 5, the coasting mode, neither the electric motor nor the combustion engine are providing power. Finally, in the recuperation mode (Mode 6), kinetic energy of the vehicle is recovered in deceleration phases. In all six operating modes, the ICE is running to supply the mechanical auxiliaries with the required power.

In Fig. 2, the simulation structure reflecting the system architecture according to Fig. 1 is depicted. Only the main effects—contributing to the longitudinal dynamics of the power train—are modelled. The individual blocks represent the component models of the hybrid system. For each component, low-order models

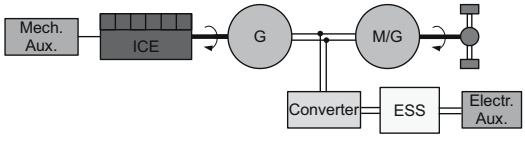

Fig. 1. Architecture of a hybrid diesel-electric railway vehicle.

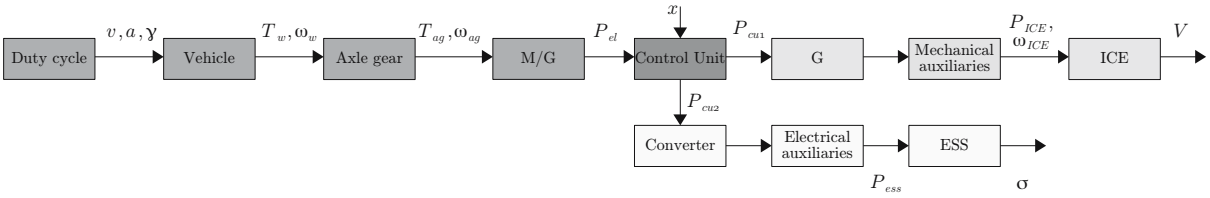

Fig. 2. Simulation structure of a diesel hybrid railway vehicle.

based on dynamic equations and static characteristic maps were derived and implemented in Matlab/Simulink. The arrows represent the numerical evaluation order of the components and not the directions of the power flow.

Note that this evaluation order is opposed to the direction of the power flow corresponding to an inverse problem setting. Therefore, the inputs of the simulation approach are the velocity and altitude profiles, whereas the outputs are given by the load points and the fuel consumption of the ICE and the state of charge (SOC) σ of the ESS (cf. Guzzella and Sciarretta, 2005). According to the control strategy, the control unit distributes the requested power for tracking the duty cycle between the ICE and the ESS. In the following section, a short description of the component models is given. The model of the converter is represented, for the sake of simplicity, by a constant efficiency factor.

2.1. Vehicle. The vehicle model results from a balance of forces

$$F_w = m_{veh} \cdot a + F_{res} + F_{inc}\,, \tag{1}$$

where F_w denotes the force at wheel, m_{veh} the mass of the vehicle, a the acceleration of the vehicle, F_{res} the resistance forces which include the air resistance and rolling resistance, and $F_{inc} = m_{veh} \cdot g \cdot \sin(\gamma)$ the inclination force with the inclination angle γ. To consider the rotary inertia of the power train, the vehicle mass m_{veh} includes the rotating masses $m_{rot} = p_{rot} \cdot m_{tare}$, $0 < p_{rot} < 1$, which are defined by the tare weight m_{tare} of the train. With the wheel diameter d_w and the velocity v of the train, the torque at wheel T_w and the rotational speed ω_w of the wheels can be calculated by

$$T_w = F_w \frac{d_w}{2}, \quad \omega_w = 2\frac{v}{d_w}. \tag{2}$$

2.2. Axle gear. The axle gear transmits the power from the drive shaft to the wheels. Corresponding to the constant gear ratio i_{ag}, the torque T_{ag} and the angular velocity ω_{ag} at the mechanical input of the axle gear can be computed by

$$T_{ag} = \frac{T_w}{i_{ag} \cdot \eta_{ag}^d}, \quad \omega_{ag} = \omega_w \cdot i_{ag}\,. \tag{3}$$

The efficiency η_{ag} of the gear box is assumed to be constant. The exponent d has to be chosen according to the direction of the power flow. For a positive power flow, directed from the propulsion system to the wheels, its value is $d = 1$. In the case of a negative power flow (for a power flow in the opposite direction), a negative exponent $d = -1$ is used.

2.3. Internal combustion engine. The ICE, which is directly connected to the electric generator, represents the prime mover of the system architecture. In the simulation model, mainly the fuel consumption V of the ICE is predicted by a measured static map of the specific fuel consumption b_e (Fig. 3). With the simulation inputs, the angular velocity ω_{ICE} and the requested ICE power P_{ICE}, the specific fuel consumption b_e is computed by using a 2D-interpolation inside the static engine map. The

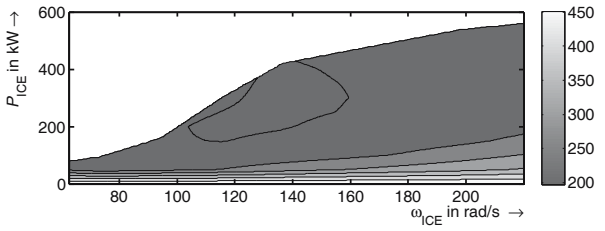

Fig. 3. Specific fuel consumption b_e in g/kWh depending on the angular velocity ω_{ICE} and the power P_{ICE}.

total fuel consumption for the ICE becomes

$$V(t) = \int_0^t \frac{P_{ICE}(\tau) \cdot b_e(\tau)}{\rho_{fuel}}\,\mathrm{d}\tau\,, \tag{4}$$

where ρ_{fuel} denotes the density of the fuel.

2.4. Electric motor/generator. The electrical drive represents a classical motor/generator unit, e.g., an induction machine. It is used either as a traction motor to move the train vehicle or as a generator to recuperate the braking energy.

By multiplication of the simulation block inputs T_{MG} and ω_{MG}, the mechanical power P_{MG} can be obtained. Depending on the direction of the power flow

($d = 1$: positive power flow; $d = -1$: negative power flow), the electric power P_{el} can be computed as

$$P_{el} = \frac{P_{MG}}{\eta_{MG}^{d}} . \tag{5}$$

The efficiency η_{MG} is determined by a linear 2D-interpolation in the efficiency map of the electric motor/generator (Fig. 4).

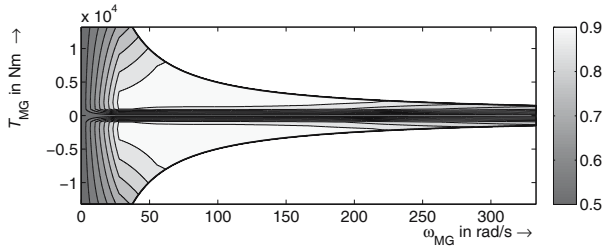

Fig. 4. Efficiency η_{MG} of the M/G depending on the rotational speed ω_{MG} and the torque T_{MG}.

2.5. Battery. A lithium-ion battery consisting of $n_{par} = 6$ branches in electric parallel connection, where each branch itself contains $n_{ser} = 216$ cells in serial connection, is used as the energy storage device. In traction phases, it provides power to the electric motor, whereas it stores the recuperated energy in braking phases. The simplified model of the battery is derived at the cell level on the basis of the work of Rauh and Aschemann (2012) for the equivalent electrical circuit of the battery illustrated in Fig. 5. It consists of a state-of-charge-controlled voltage source U_{oc} in series with a constant resistance R_{ser} representing ohmic losses.

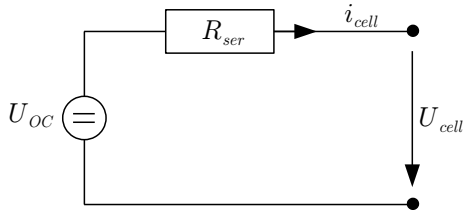

Fig. 5. Equivalent electrical circuit for the battery.

The terminal voltage U_{cell} of the cell is defined by the cell current

$$i_{cell} = \frac{P_{el}}{n_{par} \cdot n_{ser}} \cdot \frac{1}{U_{cell}} \tag{6}$$

according to

$$U_{cell} = U_{oc} - R_{ser} \cdot i_{cell} . \tag{7}$$

Using (6) and (7), the output variables U_{bat} and i_{bat} can be formulated as

$$U_{bat} = U_{cell} \cdot n_{ser}, \quad i_{bat} = i_{cell} \cdot n_{par} . \tag{8}$$

The state of charge σ results from the cell current i_{cell}, its initial value $\sigma_{init} = \sigma(0)$, and the nominal capacity C_{nom} of one cell

$$\sigma(t) = \sigma(0) - \int_0^t \frac{i_{cell}(\tau)}{C_{nom}} \, \mathrm{d}\tau . \tag{9}$$

To avoid an overheating of the battery, it is necessary to meet the maximum charging and discharging power given by the battery manufacturer. Usually, the maximum continuous power P_{cont} of the battery depends on the state of charge and allows for short phases, where power peaks exceeds the continuous power P_{cont}. Here, a three-stage limitation is employed for the maximum discharging power $P_{dch,\max}$ according to

$$P_{dch,\max} = \begin{cases} P_{peak,1} & \text{if} \quad cnt < t_1, \\ P_{peak,2} & \text{if} \quad t_1 \le cnt < t_2, \\ P_{cont} & \text{otherwise.} \end{cases} \tag{10}$$

The counter is increased in every time step by the sample time as long as the requested power P_{ess} for the ESS is larger than the continuous power P_{cont}. A reset is performed if a change from charging to discharging or the other way round occurs. The limiting values for the peak power $P_{peak,1}$ and $P_{peak,2}$ restrict the maximum discharging power for the following simulation step corresponding to the boundaries t_1 and t_2 of the counter cnt. For the charging power, an analogous approach is implemented.

2.6. Double layer capacitor. As high-power energy storage, the double layer capacitor (DLC) is used. The modelling is based on a simplified electrical circuit consisting of an internal resistance R_{DLC} in series with a capacitor C_{DLC}. Both are in parallel to a self-discharging resistance R_{dch}; see Fig. 6. The losses caused by the

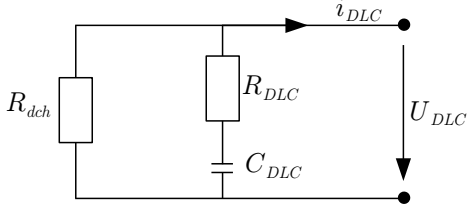

Fig. 6. Electrical circuit of the DLC.

self-discharging resistance R_{dch} were neglected because of the large value of R_{dch} and the requested duty cycle

with short steady-state times. With the requested power P_{DLC} as simulation input and the DLC voltage U_{DLC} the current results from

$$i_{DLC} = \frac{P_{DLC}}{U_{DLC}}. \tag{11}$$

A positive value of i_{DLC} corresponds to a discharging, a negative value to a charging of the DLC. The DLC voltage follows from

$$U_{DLC} = \frac{Q_{DLC}}{C_{DLC}} - R_{DLC} \cdot i_{DLC}\,, \tag{12}$$

where Q_{DLC} denotes the electric charge of the DLC. With the energy content $E_{DLC} = \frac{1}{2} C_{DLC} U_{DLC}^2$, the minimum energy content $E_{\min}$ and the usable energy content E_{use}, the state of charge σ can be calculated by

$$\sigma = \frac{E_{DLC} - E_{\min}}{E_{use}}. \tag{13}$$

The maximum discharging and charging current are limited similarly to the power limitation of the battery. If the current i_{DLC} exceeds a defined limit i_{lim} for a longer time period, the maximum current is limited for a specified period. Furthermore, the root mean square of the current i_{rms} is build on-line for a fixed number N of samples in the past

$$i_{rms} = \sqrt{\frac{\sum\limits_{t-N\cdot\Delta t}^{t} i_{DLC}^2}{N}}. \tag{14}$$

If this value exceeds a certain value, the maximum current is limited until the root mean square falls below another threshold.

3. Simulation scenario

The vehicle considered is a three-coach DMU operated as regional train, with one propulsion unit per coach (Fig. 1). Here, an increased vehicle mass accounts for the additional system components of a hybrid system architecture such as the electric motor and the ESS. The auxiliaries are characterised by a constant power demand, half of which has to be provided by the ICE and half by the ESS. As a result, the ICE is operated permanently during the whole operating time. In the case of the DLC architecture all auxiliaries are mechanical. The DLC is only used to support the ICE during traction.

As mentioned before, the velocity profiles serve as simulation inputs. Because of a calculation in the opposite direction of the power flow, it is essential that they comply with the maximum traction forces of the power train. For that purpose, the driving cycles are computed as shown by Leska *et al.* (2013) with respect to the current system architecture. All profiles are calculated with a time contingency of 10% in comparison with a time-optimal driving strategy to allow for a reduction of the fuel consumption and emissions. Figure 7 shows the resulting speed profiles for both system architectures: the one with a battery, and the other with a DLC.

In the top panel, the speed profile is shown, whereas the corresponding inclination profile, which is typical for the low mountain range of Germany, is depicted in the bottom panel.

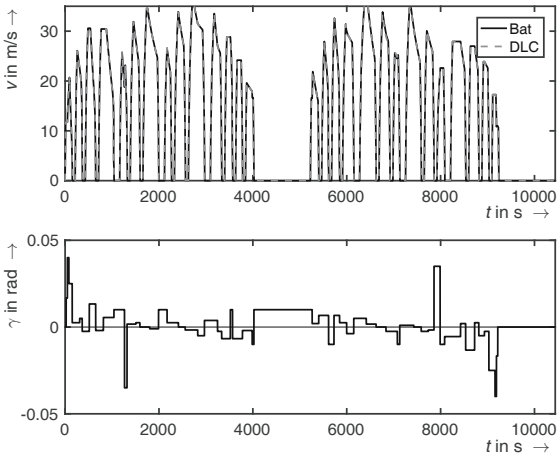

Fig. 7. Reference trajectory.

These profiles are used as simulations inputs in the following simulations.

4. Optimal operating strategy

An operating strategy for a hybrid vehicle specifies the allocation of the demanded traction power P_{el} among the propulsion systems (the ICE and the ESS). It includes a systematic approach to determining the required operating modes and control variables. For that purpose, the power split ratio x is introduced which allows for splitting the required traction power P_{el} between the ICE (P_{cu1}) and the ESS (P_{cu2}). In Mode 3, the power values of P_{cu1} and P_{cu2} are defined as

$$P_{cu1} = (1 - x) \cdot P_{el}, \quad P_{cu2} = x \cdot P_{el}\,, \tag{15}$$

with $x \in [0, 1]$. If Mode 4 (load level increase) becomes active, the power values are calculated by

$$\begin{aligned} P_{cu1} &= -x \cdot (P_{\max} - P_{el}) + P_{el}, \\ P_{cu2} &= P_{el} - P_{cu1}\,, \end{aligned} \tag{16}$$

where the power split ratio is defined as $x \in [-1, 0]$ and $P_{\max}$ denotes the maximum recuperation power, which is limited by the maximum ICE power and the maximum power of the ESS.

By adjusting the power split ratio x in an optimal way for each time step of the duty cycle, the fuel-optimal operating strategy can be found. In the following sections, two optimisation approaches are applied to the given simulation models to obtain an optimal sequence of the power split ratio x. To allow for a comparison of the achievable fuel savings of the hybrid railway vehicle, a simulation with a classical diesel vehicle is performed. The resulting fuel consumption is employed as a reference V_{ref} for the following optimisation results with the hybrid vehicle.

4.1. Bellman's dynamic programming. The dynamic programming approach according to Bellman (2003) is a computationally expensive algorithm calculating the optimal control sequence for each time step. The algorithm determines the optimal control sequence on a chosen grid backwards in time based on Bellman's optimality principle: "Regardless of the decisions taken to enter a particular state in a particular stage, the remaining decisions made for leaving that stage must constitute an optimal policy" (Bellman, 1952). The resulting operating strategy is characterised by frequent switches in the power split ratio x, but the results can be regarded as the global optimum. In general, dynamic programming is used to calculate the optimal control sequence for multi-stage decision processes.

First, the optimisation problem is discretised into $k \in \{0, \ldots, N\}$ with N time intervals, in $i \in \{1, \ldots, I\}$ with I values for the state of charge σ and in $j \in \{1, \ldots, M\}$ with M values for the power split ratio $x^j(k) \in [-1, 1]$. The resulting state of charge

$$\sigma(k+1) = f(\sigma^i(k), x^j(k)) \tag{17}$$

and the actual costs (fuel consumption)

$$V_0(k) = g(\sigma^i(k), x^j(k)) \tag{18}$$

are then computed in for each decision k using the simulation model given in Fig. 2. Hence the minimum costs $V^{N-(k+1)}$ for the remaining trajectory can be obtained for all states $\sigma^i(k)$ by solving the following optimisation problem:

$$V^{N-k}(\sigma^i(k)) = \min_{x^j(k)} \{V_0(\sigma^i(k), x^j(k)) + V^{N-(k+1)}(\sigma(k+1))\}, \tag{19}$$

where $V^{N-(k+1)}(\sigma(k+1))$ denotes the remaining costs starting from the resulting state $\sigma(k+1)$ up to the final stage N.

The dynamic programming starts at the stage $k = N-1$ and is evaluated according to Bellman's optimality principle backwards in time until the first stage $k = 0$ is reached. For that purpose, at first, the load points (P_{el}) corresponding to the duty cycle—characterised by the velocity profile as well as the inclination profile—are identified off-line for every time step k by evaluating the grey shaded components of the simulation model in Fig. 2. With the load point (P_{el}) and the initial state of charge $\sigma^i(k)$, the resulting state of charge $\sigma(k+1)$ and the actual costs $V_0(k)$ can be computed. If the resulting state of charge $\sigma(k+1)$ is not equal to one of the N discrete values of the state of charge $\sigma^{i(k+1)}$, the remaining costs $V^{N-(k+1)}$ will be determined by an interpolation between the two closest states of charge. The overall costs for all N time intervals can be calculated by

$$V^N(x(0)) = \sum_{k=0}^{N-1} (V_0(\sigma(k), x(k)) + V(x(N))). \tag{20}$$

4.1.1. Battery. For the given system architecture with an on-board battery, the optimisation problem is discretised into $N = 11079$ time steps, $I = 1001$ values for the state of charge $\sigma \in [0.4, 0.6]$ and $M = 201$ values for the power split ratio x. Figure 8 shows the resulting progression of the state of charge $\sigma(t)$ and the corresponding progressions of the requested power P_{el}, the power values for P_{cu1} and P_{cu2} and the maximum discharging and charging power $P_{cu2,\max}$ and $P_{cu2,\min}$, which include the power limitations of all relevant components, e.g., the battery, the generator and the ICE.

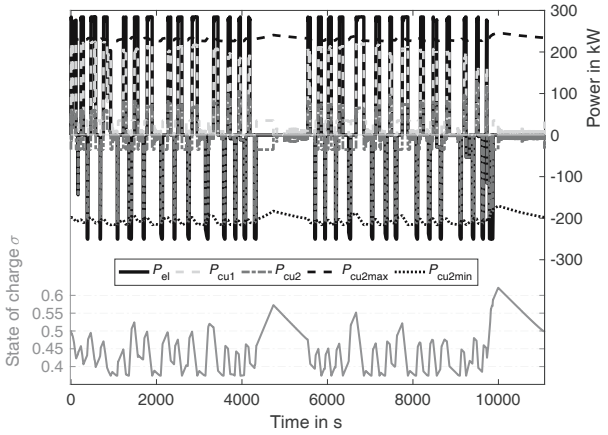

Fig. 8. Optimisation results by dynamic programming for the hybrid vehicle with a battery ESS.

The state of charge of the battery at the starting point is equal to the one at the final destination. This is demanded for all optimisation experiments in this article to ensure a fair comparison with the standard diesel vehicle. Compared with the standard railway vehicle, a fuel saving of 24% could be achieved. Regarding

the large values of P_{cont} (see (10)), for the state of charge values above $\sigma = 0.4$, the power restrictions caused by the counter (see Section 2), are not relevant here. Hence the results by dynamic programming can be seen as a global optimum disregarding the numerical and the discretisation errors. The frequent switchings in the power values shown in Fig. 8 are typical for the dynamic programming approach. This effect and, especially, the high computational effort inhibit the use in an on-line operating strategy.

4.1.2. DLC. For the system architecture with an on-board DLC, a fuel saving of 17% is achieved compared with the standard diesel vehicle. The optimisation problem is discretised into $N = 11079$ time steps, $I = 251$ values for the state of charge $\sigma \in [0, 1]$ and $M = 201$ values for the power split ratio x. Figure 9 shows the resulting progression of the state of charge $\sigma(t)$ and the corresponding progressions of the power values for P_{el}, P_{cu1}, P_{cu2}, $P_{cu2,\max}$ and $P_{cu2,\min}$.

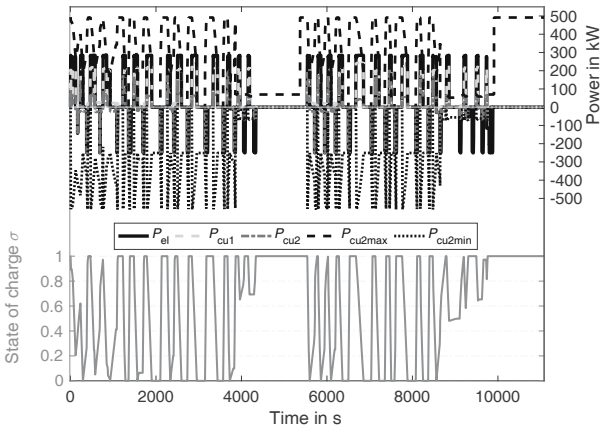

Fig. 9. Optimisation results by dynamic programming for the hybrid vehicle with a DLC ESS.

The progression of the state of charge is balanced between the starting point and the final destination as demanded. At the time periods from 3800 to 5500 s and from 8800 to 10000 s, a significant reduction in the maximum charging $P_{cu2,\min}$ and discharging power $P_{cu2,\max}$ caused by the root mean square i_{rms} can be observed; see Section 2. Such methods which are based on counters cannot be considered in the dynamic programming because of the calculation in the backward direction. It cannot be definitely said if the obtained results could be seen as a global optimum.

4.2. Sensitivity analysis optimisation. To compare and to assess the results of the dynamic programming, a second optimisation approach is applied to the two hybrid problems. The so-called sensitivity analysis optimisation by Leska *et al.* (2014) is used. This approach calculates the optimal operating strategy of hybrid vehicles in two steps. First, characteristics of the optimal power split ratios x in Modes 3 and 4 are computed by a sensitivity analysis. Afterwards, these characteristics serve for calculating the fuel optimal operating strategy using adequate optimisation approaches.

If the grey-shadowed blocks in the simulation model in Fig. 2 are neglected, the optimal power split ratios x are calculated by a numerical sensitivity analysis of the remaining simulation structure. Different load points (P_{el}^i) are applied as inputs. For $k \in \{1, \ldots, 100\}$, simulations are performed with a specified initial state of charge of σ_{init}, a fixed simulation time and varying values of x_k^i to determine the corresponding fuel consumptions V_k^i and thresholds for σ_k^i. With the simulation results V_d^i and σ_d^i for a pure diesel drive ($x_k^i = 0$) the optimal power split ratios $x_k^i \in [0, 1]$ in Mode 3 can be determined by the evaluation of the boost sensitivity s_b according to

$$s_b^i = \left\{ \frac{V_d^i - V_k^i}{\sigma_d^i - \sigma_k^i} \right\} \cdot 100\,. \tag{21}$$

The higher the boost sensitivity s_b^i, the more efficient is the support of the diesel engine by the ESS at the current load point (P_{el}).

Analogously, the optimal power split ratios $x_k^i \in [0, 1]$ in Mode 4 can be determined by the evaluation of the load increase sensitivity s_l according to

$$s_l^i = \left\{ \frac{V_k^i - V_d^i}{\sigma_k^i - \sigma_d^i} \right\} \cdot 100\,. \tag{22}$$

It indicates the additional fuel consumption for charging the battery by one percent of its usable energy content. The lower the load increase sensitivity s_l, the more efficient is the load increase mode at the current load point (P_{el}).

4.2.1. Battery. Figure 10 shows the boost sensitivities for the system architecture with an on-board battery. As mentioned before, the larger these sensitivities, the higher is the potential to save fuel. The best boosting conditions are obtained at high loads with a small power split value x. However, they get worse with increasing power split ratios x and decreasing loads.

The load increase sensitivities for the battery are depicted in Fig. 11. In the white region, the power P_{cu2} is too small to supply the electrical auxiliaries, which leads to a decreasing state of charge.

It is not meaningful to use Mode 4 in this area. The promising scenarios for a load increase—characterised by small sensitivities s_l—are related to small loads P_{el} and power split ratios x. With increasing loads as well as power split ratios, the costs increase.

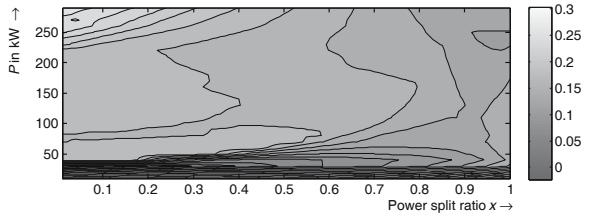

Fig. 10. Boost sensitivities s_b for the battery.

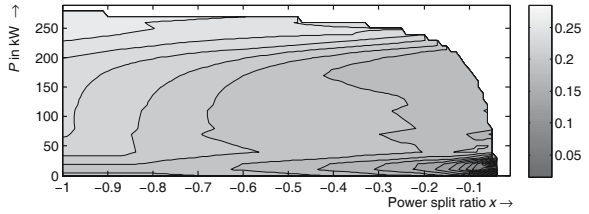

Fig. 11. Load increase sensitivities s_l for the battery.

In the work of Leska *et al.* (2014), the fuel optimal operating strategy is determined by the introduction of an additional parameter s_{lim} that defines the minimum value for s_b. Accordingly, Mode 3 is only used at load points with a power split ratio x larger than $s_{b,lim}$. At load points with a boost sensitivity $s_b < s_{b,lim}$, any boosting is omitted. The optimal strategy can be evaluated by a bisection method. In every iteration step, one complete simulation is performed for a certain factor of $s_{b,lim}$ until the state of charge at the final destination is equal to the one at the starting point; see Fig. 12.

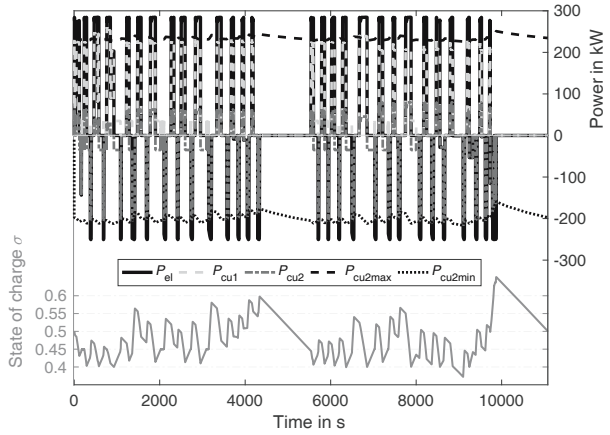

Fig. 12. Optimisation results by sensitivity analysis optimisation for the hybrid vehicle with a battery ESS.

To limit the range of the state of charge σ, the bounds are implemented in the simulation model. Consequently, any boosting is performed below $\sigma \leq 0.4$ and no load increase is used if $\sigma \geq 0.6$. During recuperation, however, σ is allowed to exceed the upper bound. The lower bound may be violated in some periods due to the auxiliaries. In addition to $s_{b,lim}$, an additional parameter $s_{l,lim}$ is introduced to allow for a load increase—especially at small loads including zero. In the given scenario, however, the sensitivities s_l are quite small in comparison with the boost sensitivities. The optimisation is subject to an interlaced structure according to the following algorithm:

repeat: specification of $s_{l,lim}$ (golden section method)

repeat: specification of $s_{b,lim}$ (golden section method)

- execution of a simulation run
- optimization of $s_{b,lim}$ in sections where the minimum SOC value $\sigma_{\min}$ is attained
- evaluation of the corresponding cost function value

until the terminal criterion is fulfilled

until the terminal criterion is fulfilled.

In the outer loop, the optimal parameter $s_{l,lim}$ is determined by a golden section search. Using a golden section search as well, $s_{b,lim}$ is adjusted in the inner loop. In each section, where Mode 3 is terminated by the lower bound of the state of charge, the thresholds of $s_{b,lim}$ are increased as long as the minimum value of σ is still at the lower bound. The resulting progression of the state of charge and the corresponding power are shown in Fig. 12. Compared with the standard diesel vehicle, a fuel saving of 23% could be achieved. This result is very close to the one of the dynamic programming representing (at least theoretically) the global optimum; advantageously, the former approach strongly reduces the computational effort.

4.2.2. DLC. The boost sensitivities for the architecture with a DLC are depicted in Fig. 13. Accordingly, the favourable boost situation—as for the battery—corresponds to high loads P_{el} at small power split ratios x. In general, the sensitivity values are smaller than those for the battery due to a smaller capacity.

Figure 14 shows the load increase sensitivities for the DLC architecture. The most promising areas—with small sensitivities s_l—are at low loads P_{el} and small values of x.

Given these characteristics, the optimal operating strategy can be determined by means of the thresholds $s_{b,lim}$ and $s_{l,lim}$. In contrast to the dynamic programming approach, the power limitations of the DLC can be addressed here. The algorithm can be summarized as follows where the condition $\max(i_{rms}(t)) < i_{rms,\max}$ must be always fulfilled:

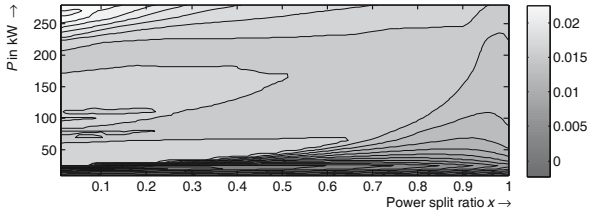

Fig. 13. Boost sensitivities s_b for the DLC.

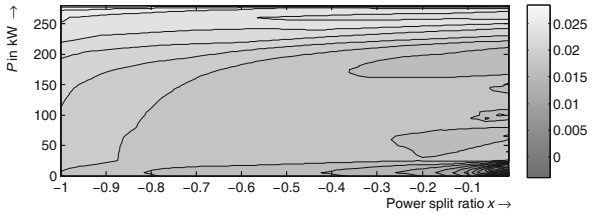

Fig. 14. Load increase sensitivities s_l for the DLC.

repeat: bisection of $s_{b,lim}$

- reduction of the generator power during sections with $\sigma_{end} = 1$ by lowering $i_{rms}(t)$
- increase of $s_{b,lim}$ in sections with $\sigma_{end} = \sigma_{\min}$ (see also Section 4.2.1)

until $i_{rms,\max} - \max(i_{rms(t)}) < \epsilon$, where $\epsilon > 0$

repeat: golden section method for $s_{l,lim}$ within sections with $\sigma_{end} < 1$

- selection of $s_{b,lim}$ and simulation

until the terminal criterion is fulfilled.

The main indicator for a power limitation is the root mean square value i_{rms}, which is based on the last time steps. If this value exceeds a predefined threshold, the power will be limited until it comes back to a fixed value. To consider the value of i_{rms}, the optimisation is performed in two steps: Firstly, the threshold of $s_{b,lim}$ will be adjusted by means of a bisection method as long as no power limitations occur, which means that i_{rms} does not exceed the maximum value. In every iteration step, one simulation is performed for a certain value of $s_{b,lim}$. To avoid any power limitation of the DLC, two additional adoption methods are used: On the one hand, the braking power of the electric motor/generator is reduced in sections where the DLC is completely charged at the end. This reduces the root mean square value i_{rms}. On the other hand, the threshold of $s_{b,lim}$ is adjusted in sections where the DLC is completely discharged. It is increased as long as the DLC stays completely discharged to prefer more efficient power split ratios x.

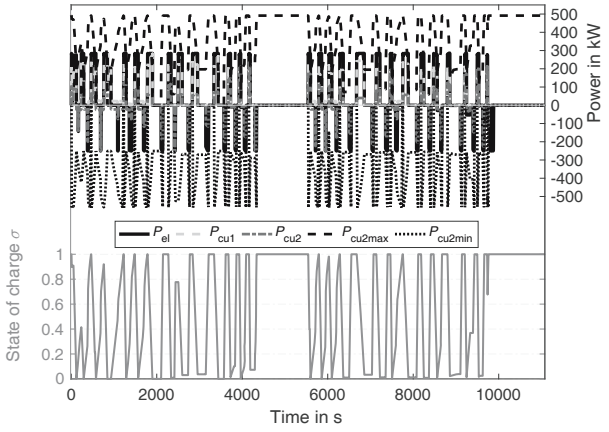

Fig. 15. Optimisation results by sensitivity analysis optimisation for the hybrid vehicle with a DLC.

Secondly, the load increase mode is introduced in sections with an incompletely charged DLC at the end. Only sections are considered where an increasing value of i_{rms} does not lead to exceeding its bounds. The power split value is defined by the load increase sensitivity $s_{l,lim}$, which is adjusted by a golden section search. In every iteration, one simulation is performed and the adoption methods mentioned before are applied. Furthermore, the threshold of $s_{b,lim}$ is decreased in the corresponding sections to use the additional energy generated by the load increase. The resulting progression of the DLC charge is shown in Fig. 15. It is well visible that no power limitation occurs. The DLC charge is balanced over the duty cycle and the fuel saving compared to the diesel vehicle comes to 18.3% which means 1.3% more than by dynamic programming.

5. Discussion

5.1. Comparison of dynamic programming and sensitivity analysis optimization. In Section 4, two optimization approaches are presented and applied to calculate the fuel-optimal operating strategy for a diesel hybrid railway vehicle with a battery and a DLC as on-board energy storage. The resulting fuel-savings in comparison with the standard diesel vehicle are summarized in Table 1. In general, dynamic programming is used to calculate the optimal control sequence for discrete multi-stage decision processes. If an adequate discrete approximation of the continuous system exists, the results of the dynamic programming can be seen as a global optimum up to numerical and discretization errors. In the present article, current and power restrictions depending on their previous progressions are relevant for both energy storages; see Section 2. Due to a calculation backwards in time, however, dynamic programming

cannot address these limitations. If they are attained, it is no longer guaranteed that the results of dynamic programming provide a global optimum.

As the SOC of the battery is always kept above a certain level in this optimization, the power limitations of the battery do not affect the operating strategy. In this area, the battery is able to provide enough power, even if only the continuous power P_{cont} is usable. Consequently, the results of the dynamic programming for the battery can be seen as a global optimum. In comparison with this result, the sensitivity analysis optimisation achieves similarly good results.

In the case of the DLC, the limitations—which are related to the root mean square value of current i_{rms}—do affect the operating strategy. Here, dynamic programming does not provide any more the global optimum, and the sensitivity analysis approach produces better results.

Table 1. Optimization results.

	Battery	DLC	Computing time
DP	24%	17%	13476 s
SO	23%	18%	2 s

In addition to the fuel savings, the required computing time is stated in Table 1. Computation with an Intel Core i7 2.70 GHz computer of the fuel-optimal operating strategy for the hybrid vehicle with a battery took 13476 s with the dynamic programming and 2 s with the sensitivity analysis optimisation. Here, the computation time for the calculation of sensitivity characteristics is neglected. They are related to the system architecture and have to be determined only once.

The computing times indicate that the dynamic programming is not very promising for the use in an on-line energy management strategy such as model predictive control. The calculation takes a lot of time and could be done only for small prediction horizons or for highly simplified models in a sufficiently small time period. By contrast, the sensitivity analysis optimisation in contrast needs much less time than dynamic programming. Only one parameter has to be adopted to determine the fuel-optimal operating strategy. In combination with a prediction of the future speed profile, this approach is very promising for the usage in an on-line energy management.

5.2. Life cycle costs. The investment decision process for the selection of a traction system for a railway vehicle is often based on the so called *life cycle costs* (LCCs), which includes the initial costs, the running costs for fuel, and the maintenance costs for a specified time period. As all the system architectures considered use the same diesel engine, the initial and maintenance costs for this engine are the same. Only the initial and maintenance costs for additional system components of the hybrid vehicle, especially for the energy storage, have to be considered. Furthermore, lifetime aspects of the energy storage systems have to be included in the life cycle costs. If the usable lifetime is less than the one of the vehicle and the covered LCC period of 20 years, the energy storage has to be replaced, and the additional investment costs have to be added to the LCC costs. For batteries and DLCs, usually not the whole system has to be replaced, but only the storage modules, which results in lower replacement costs in comparison with the initial costs. Hence the dominant factors for the LCC are the costs for the fuel and the energy storage system.

5.3. Fuel costs. The fuel costs are one of the dominating elements in the LCC assessment. They result from the total fuel consumption during the LCC period and the corresponding fuel price. This is mainly governed by the world crude oil price and the tax regulations of the countries. It changes not only from country to country but also in time. This makes it very difficult to convert the fuel savings in Table 1 into costs, which is necessary to compare it with the additional investment costs. Therefore, the average value $c_{fuel,av}$ of a specified fuel price scenario is usually used to calculate the fuel costs for the LCC period.

5.4. Energy storage costs. The costs for the energy storage system are composed of the initial and replacement costs, which become relevant if the lifetime of the ESS is shorter than the LCC period. The lifetime of the energy storage system mainly depends on the ageing characteristics.

5.5. Ageing of a double layer capacitor. Double layer capacitors belong to a category between batteries and conventional capacitors. Due to low internal resistances, they are able to accept and provide high power levels. The process of charging is nearly reversible. They are characterised by a high cycle stability, a high power density and mechanical robustness. Thus, they are typically used in applications with high power requests in short time periods, such as hybrid vehicles. However, their capacitance reduces over their lifetime. Even though the energy storage in a DLC is pure electrostatic, parasitic electrochemical reactions occur (Bohlen *et al.*, 2007a; 2007b). Chemical mechanisms as well as processes of physical nature (Bittner *et al.*, 2012) are expected to change the structural characteristics of the electrodes and the chemistry of the electrolyte. These effects are mainly influenced by the temperature and voltage. The higher these values, the more the electrochemical reactions will be accelerated. The impact of this degradation can be

described by an increase in the internal resistance and a decrease in the capacitance.

According to the investigations reported by Bohlen *et al.* (2007a; 2007b), the main part of the ageing arises from the calendric ageing and not from the cyclic ageing. Hence, the operating strategy can only influence slightly the ageing behaviour of the DLC. The lifetime of the DLC is reached if the capacitance has reached a value of 80% of the nominal one. For a DLC in traction applications, the calendric lifetime is predicted to be maximally 15 years. This means that the DLC has to be replaced once in the LC period of 20 years. Consequently, the LCC costs are given by the sum of the fuel costs, the initial costs of the DLC and the replacement costs. If these costs are smaller than the fuel costs of the conventional diesel vehicle, the hybrid vehicle is cheaper.

5.6. Ageing of a battery. Beside specific energy, energy density, specific power, safety, recyclability and costs, the cycle life is one of the most important properties of a traction battery (Lorf, 2013). It is limited due to degradation and ageing of the battery, which are related to electrochemical phenomena, which change the materials and the properties of the battery cell. Ageing starts in the chemical composition of the battery's electrolyte and goes on with degradation mechanisms at the electrodes (Barré *et al.*, 2013), whereas the origin can be either mechanical or chemical. The effects of the ageing can be described by a capacity fade and an increase in the internal resistance (Waag *et al.*, 2013). A distinction is made between calendric ageing and cyclic ageing (Meissner and Richter, 2005). The sum of both effects represents the overall ageing of battery.

Calendaric ageing refers to the irreversible part of the lost capacity by battery storage (Sarre *et al.*, 2004). It is mainly influenced by the storage temperature (Omar *et al.*, 2014) and the SOC level during storage (Ohue *et al.*, 2011). These parameters cannot be directly influenced by the operating strategy. According to the manufacturer's data, the battery cell reaches a calendric age of 20 years at $20°$C and 10 years at $40°$C. Under these circumstances, it is expected that the battery cells have to replaced once within the LCC period.

Cyclic ageing occurs during the charging and discharging phases of the battery. It depends on parameters such as cycling depth, charge volume, maximum SOC and depth of discharge (DOD), mean discharge and charge current (see Herb, 2010). All of them are related to the chemistry and the construction of the battery and to the operating strategy, respectively. In the work of Marongiu *et al.* (2015), the influence of the vehicle-to-grid strategy on the ageing behaviour of lithium ion batteries is investigated. It was figured out that the chemistry plays an important role. The impact of the special design is investigated by Rothgang *et al.* (2015). It is shown that a modular energy storage system can lead to a higher flexibility in the system design and enhance lifetime and safety at the same time. In the work of Lorf (2013), it is shown that the optimum size of a battery for an electric vehicle depends on the system architecture and the speed profile but also on the battery degradation. With increasing cycle numbers the available capacity as well as the available power fades. In order to satisfy the power requirements at the end of the LCC period, it is necessary to consider a certain spare capacity at the beginning. This leads to an optimum battery capacity of around 1.25 to 1.75 times the optimal nominal battery capacity and increases the initial costs.

Another way to influence cyclic ageing is to adopt the operating strategy in order to maximise the battery lifetime. For this purpose, the ageing has to be estimated and the additional replacement costs have to be considered in the performance index. To evaluate ageing, several indicators are proposed to quantify the health level of the battery (Barré *et al.*, 2013). The most common is the *state of health* (SOH), which is defined by

$$SOH = \frac{\text{nominal capacity at } t}{\text{initial capacity}}. \tag{23}$$

Various methods exist for SOH estimation, which can be divided in five groups (Barré *et al.*, 2013):

- electrochemical models,
- equivalent-circuit-based models,
- performance-based models,
- analytical models with empirical fitting,
- statistical approaches.

Each of these methods tries to solve the ageing estimation problem, and is subject to individual pros and cons. One method, the rainflow counting algorithm (Meissner and Richter, 2005), only considers the number of cycles and the corresponding cycle depth. Under the assumptions that the order of the loading makes no difference and that the damage accumulation is independent of the stress level this algorithm counts the number of cycles and separates them according to their magnitude. The results are the mean value, the amplitude and the number of repetitions of the oscillation. Usually, the end of life of a battery is reached if the capacity is dropped by 20%. In general, the manufacturers provide the dependency of the maximum number of cycles for different depths of decharge (DODs) in a cycle life curve. According to this curve, the lifetime of the battery is reached if

$$D = \sum_{i=1}^{N} \frac{n_i}{n_{\max,i}} = 1. \tag{24}$$

Here, the sum of the relation between n_i, the number of cycles with the i-th DoD, and $n_{\max,i}$, the maximum number of cycles with the i-th DOD, are built for all N occurring DODs. Accordingly, the maximum number of years n_y of the battery can be calculated on the basis of one journey of the train with the driving time t_f and the operating time per year T by

$$n_y = \frac{t_f}{T \cdot D}. \tag{25}$$

The operating hours per year vary from train to train and from year to year. It is not possible to state an accurate value for the operating time. Hence, the average value of $T = 3500\ \mathrm{h/a}$ is assumed. With this value, the lifetime $n_y = 8.2\ \mathrm{a}$ of batteries is calculated by the rainflow counting algorithm.

6. Conclusions

In this article, a comparative calculation of a hybrid diesel-electric railway vehicle with two different energy storage systems has been presented. On the one hand, a lithium-ion battery is used as an example for a high-energy ESS. On the other hand, a double layer capacitor is investigated representing a high-power ESS. The sizes of both the storages are chosen in agreement with the maximum weight of the train. Based on the control-oriented model presented in this paper and the track specifications, two different optimisation approaches are applied and compared with each other. Bellman's dynamic programming according is the most common method in this area. It is computationally expensive and, hence, not applicable to an on-line operating strategy on board at trains in revenue service. Furthermore, it is not perfectly applicable to all optimisation problems. Nevertheless, if it can be employed, the results can be considered a global optimum.

As the second optimisation approach, an innovative sensitivity-based method has been proposed and adapted to the problems under consideration. The performance is close to the one using dynamic programming, although with a significantly smaller evaluation time. Since only several parameters are required to adopt the operating strategy, this approach is also very promising for an on-line power management, e.g., in model-predictive control.

Acknowledgment

This work was financially supported by the European Commission within the framework of the project *Cleaner European Rail-Diesel (CleanER-D)*, EC contract no. FP7-234338, grant no. 6316006.

References

Barré, A., Deguilhem, B., Grolleau, S., Gérard, M., Suard, F. and Riu, D. (2013). A review on lithium-ion battery ageing mechanisms and estimations for automotive applications, *Journal of Power Sources* **241**: 680–689.

Bellman, R. (1952). On the theory of dynamic programming, *Proceedings of the National Academy of Sciences of the USA* **38**(8): 716–719.

Bellman, R. (2003). *Dynamic Programming*, Dover Publications, Mineola, NY.

Bittner, A., Zhu, M., Yang, Y., Waibel, H., Konuma, M., Starke, U. and Weber, C. (2012). Ageing of electrochemical double layer capacitors, *Journal of Power Sources* **203**: 262–273.

Bohlen, O., Kowal, J. and Sauer, D.U. (2007a). Ageing behaviour of electrochemical double layer capacitors. Part I: Experimental study and ageing model, *Journal of Power Sources* **172**(1): 468–475.

Bohlen, O., Kowal, J. and Sauer, D.U. (2007b). Ageing behaviour of electrochemical double layer capacitors. Part II: Lifetime simulation model for dynamic applications, *Journal of Power Sources* **173**(1): 626–632.

Brahma, A., Guezennec, Y. and Rizzoni, G. (2000). Optimal energy management in series hybrid electric vehicles, *Proceedings of the American Control Conference, Chicago, IL, USA*, pp. 60–64.

Dittus, H., Hülsebusch, D. and Ungethüm, J. (2011). Reducing DMU fuel consumption by means of hybrid energy storage, *European Transport Research Review* **3**(3): 149–159.

Guzzella, L. (2013). Automobiles of the future and the role of automatic control in those systems, *Annual Reviews in Control* **33**(1): 1–10.

Guzzella, L. and Sciarretta, A. (2005). *Vehicle Propulsion Systems: Introduction to Modeling and Optimization*, Springer, Berlin.

He, H., Xiong, R., Zhao, K. and Liu, Z. (2013). Energy management strategy research on a hybrid power system by hardware-in-loop experiments, *Applied Energy* **112**: 1311–1317.

Herb, F. (2010). *Alterungsmechanismen in Lithium-Ionen-Batterien und PEM-Brennstoffzellen und deren Einfluss auf die Eigenschaften von daraus bestehenden Hybrid-Systemen*, PhD thesis, University of Ulm, Ulm.

Hillmansen, S. and Roberts, C. (2007). Energy storage devices in hybrid railway vehicles: A kinematic analysis, *Proceedings of the Institution of Mechanical Engineers: Journal of Automobile Engineering* **221**(1):135–140.

Hillmansen, S., Roberts, C. and McGordon, A. (2009). *DMV Hybrid Concept Evaluation*, Final report, EU project, `www.birmingham.ac.uk/Documents/college-eps/railway/HybridRailReportDMUV1.pdf`

Katranik, T. (2010). Analytical method to evaluate fuel consumption of hybrid electric vehicles at balanced energy content of the electric storage devices, *Applied Energy* **87**(11): 3330–3339.

Katrasnik, T., Trenc, F. and Opresnik, S. (2007). Analysis of energy conversion efficiency in parallel and series hybrid powertrains, *IEEE Transactions on Vehicular Technology* **56**(6): 3649–3659.

Leska, M. and Aschemann, H. (2015). Fuel-optimal combined driving strategy and energy management for a parallel hybrid electric railway vehicle, *Proceedings of the 20th International Conference on Methods and Models in Automation and Robotics, Międzyzdroje, Poland*, pp. 1127–1132.

Leska, M., Grüning, T., Aschemann, H. and Rauh, A. (2013). Optimal trajectory planning for standard and hybrid railway vehicles with a hydro-mechanic transmission, *Proceedings of the European Control Conference (ECC), Zurich, Switzerland*, pp. 4550–4555.

Leska, M., Prabel, R., Aschemann, H. and Rauh, A. (2014). Operating strategy for hybrid railway vehicles based on a sensitivity analysis, *Proceedings of the World Congress of the International Federation of Automatic Control (IFAC), Cape Town, South Africa*, pp. 942–947.

Lorf, C. (2013). *Optimum Battery Capacity for Electric Vehicles with Particular Focus on Battery Degradation*, PhD thesis, Imperial College London, London.

Marongiu, A., Roscher, M. and Sauer, D.U. (2015). Influence of the vehicle-to-grid strategy on the aging behavior of lithium battery electric vehicles, *Applied Energy* **137**: 899–912.

Meinert, M., Melzer, M., Kamburow, C., Palacin, R., Leska, M. and Aschemann, H. (2015). Benefits of hybridisation of diesel driven rail vehicles: Energy management strategies and life-cycle costs appraisal, *Applied Energy* **157**: 897–904.

Meissner, E. and Richter, G. (2005). The challenge to the automotive battery industry: The battery has to become an increasingly integrated component within the vehicle electric power system, *Journal of Power Sources* **144**(2): 438 – 460.

Moreno, J., Ortuzar, M. and Dixon, J. (2006). Energy-management system for a hybrid electric vehicle, using ultracapacitors and neural networks, *IEEE Transactions on Industrial Electronics* **53**(2): 614–623.

Ogawa, T., Yoshihara, H., Wakao, S., Kondo, K. and Kondo, M. (2007). Energy consumption analysis of FC-EDLC hybrid railway vehicle by dynamic programming, *Proceedings of the European Conference on Power Electronics and Applications, Aalborg, Denmark*, pp. 1–8.

Ohue, K., Utsunomiya, T., Hatozaki, O., Yoshimoto, N., Egashira, M. and Morita, M. (2011). Self-discharge behavior of polyacenic semiconductor and graphite negative electrodes for lithium-ion batteries, *Journal of Power Sources* **196**(7): 3604–3610.

Omar, N., Monem, M.A., Firouz, Y., Salminen, J., Smekens, J., Hegazy, O., Gaulous, H., Mulder, G., den Bossche, P.V., Coosemans, T. and Mierlo, J.V. (2014). Lithium iron phosphate based battery—assessment of the aging parameters and development of cycle life model, *Applied Energy* **113**: 1575–1585.

Ott, T., Zurbriggen, F., Onder, C. and Guzzella, L. (2012). Cycle-averaged efficiency of hybrid electric vehicles, *Proceedings of the Institution of Mechanical Engineers D: Journal of Automobile Engineering* **227**(1): 78–86.

Pisu, P. and Rizzoni, G. (2007). A comparative study of supervisory control strategies for hybrid electric vehicles, *IEEE Transactions on Control Systems Technology* **15**(3): 506–518.

Rauh, A. and Aschemann, H. (2012). Sensitivity-based state and parameter estimation for lithium-ion battery systems, *Proceedings of the 9th International Conference on System Identification and Control Problems, SICPRO'12, Moscow, Russia*, pp. 469–485.

Rothgang, S., Baumhöfer, T., van Hoek, H., Lange, T., Doncker, R.W.D. and Sauer, D.U. (2015). Modular battery design for reliable, flexible and multi-technology energy storage systems, *Applied Energy* **137**: 931–937.

Sarre, G., Blanchard, P. and Broussely, M. (2004). Aging of lithium-ion batteries, *Journal of Power Sources* **127**(1–2): 65–71.

Torres, J., Gonzalez, R., Gimenez, A. and Lopez, J. (2014). Energy management strategy for plug-in hybrid electric vehicles. A comparative study, *Applied Energy* **113**: 816–824.

Waag, W., Käbitz, S. and Sauer, D.U. (2013). Experimental investigation of the lithium-ion battery impedance characteristic at various conditions and aging states and its influence on the application, *Applied Energy* **102**: 885–897.

Wang, A. and Yang, W. (2006). Design of energy management strategy in hybrid vehicles by evolutionary fuzzy system. Part I: Fuzzy logic controller development, *Proceedings of the 6th World Congress on Intelligent Control and Automation (WCICA), Dalian, China*, pp. 8324–8328.

Maik Leska was born in Parchim, Germany, in 1982. He received his diploma degree in mechanical engineering from the University of Rostock in 2009. Then he was a PhD student at the Chair of Mechatronics at the University of Rostock until 2015. The research focus was on the development of fuel-optimal energy management strategies and model-predictive controllers for hybrid railway vehicles. Since 2015 he has been a PLM consultant at ECS GmbH in Rostock.

Harald Aschemann was born in Hildesheim, Germany, in 1966. He received his diploma degree in mechanical engineering from the University of Hanover, Germany, in 1994. After two years of work in research and development with a leading company in machine tools, where he worked on automated transfer systems, he joined the Department of Measurement, Control, and Microtechnology at the University of Ulm, Germany. He completed his PhD (Dr.-Ing.) on optimal trajectory planning and trajectory control of an overhead travelling crane in 2001. From 2001 till 2006, he proceeded as a research associate and a lecturer at the same department. Since 2006 Harald Aschemann has been a full professor and the head of the Chair of Mechatronics at the University of Rostock, Germany. His research interests involve control-oriented modelling, identification, nonlinear control, and simulation of mechatronic, robotic and thermofluidic systems. In 2011, he became a corresponding member of the International Academy of Engineering, Moscow, Russia.

Michael Melzer received his diploma in transport engineering in 2008 and his PhD degree in 2014, both from the Dresden University of Technology. Since 2012 he has been employed at Siemens AG in Erlangen. His scientific interests include modelling, development and testing of energy storage systems mainly for transport applications.

Michael Meinert graduated in electrical engineering (electrical railway systems) from the Dresden University of Technology, Germany, in 1995 and received his doctorate in electrical engineering from the Darmstadt University of Technology, Germany, in 2007. His employment experience includes Siemens AG, Erlangen (since 1995) in the field of rolling stock and railway power supply as well as the Darmstadt University of Technology (from 2001 to 2004). He is currently the head of the R&D group for energy storage units/systems as well as overhead contact line free systems at Siemens AG, Mobility. His special fields include railway systems, high temperature superconductivity and innovative energy systems.

Received: 26 February 2016
Revised: 22 September 2016
Accepted: 31 January 2017